Direct holographic imaging of ultrafast laser damage process in thin films

Nerijus Šiaulys,[1] Laurent Gallais,[2] and Andrius Melninkaitis[1,*]

[1]*Laser Research Center, Vilnius University, Saulėtekio aléja 10, LT-10223 Vilnius, Lithuania*

[2]*Institut Fresnel, Aix-Marseille Université, CNRS, Ecole Centrale Marseille, Campus de St Jérôme, 13013 Marseille, France*

**Corresponding author: andrius.melninkaitis@ff.vu.lt*

Received January 2, 2014; revised March 4, 2014; accepted March 11, 2014;
posted March 11, 2014 (Doc. ID 203724); published March 31, 2014

Dynamic process of femtosecond laser-induced damage formation in dielectric thin films is reconstructed from a series of time-resolved images. Ta_2O_5 single-layer coatings of four different thicknesses have been investigated in transmission mode by means of time-resolved off-axis digital holography. Different processes overlapped in time were found to occur; namely, the Kerr effect, free-electron generation, ultrafast lattice heating, and shockwave generation. The trends in contribution of these effects are qualitatively reproduced by numerical models based on electron-rate equations and Drude theory, which take into account transient changes in the films and interference effects of the pump and probe pulses. © 2014 Optical Society of America

OCIS codes: (090.1995) Digital holography; (100.0118) Imaging ultrafast phenomena; (140.3330) Laser damage; (310.0310) Thin films.

http://dx.doi.org/10.1364/OL.39.002164

Optical interference coatings play a key role in femtosecond (fs) laser systems. A main concern of the fs system development is limitation of fluence by optical damage. The ability to model physical mechanisms of ultrafast excitation is essential for better understanding of damage behavior in coatings. An appropriate mathematical model would bring new opportunities of material selection and layer structure optimization for increased optical resistance. However, all models should be supported by experimental evidence to assess their validity. Measurement of laser-induced damage threshold (LIDT) as a function of a particular parameter is probably the mostly used approach, thus resulting in various phenomenological laws. A time-resolved pump-probe technique is also widely used. Temporal evolution of dielectric function was probed for bulk materials [1] and optical coatings [2]. Such experiments are particularly useful to resolve temporal dynamics of the damage process. Nevertheless, without good spatial resolution, many relevant details of the interaction process remain uncovered. Only in recent years has more attention been attributed to damage morphology and time-resolved imaging of the damage process. Postmortal observation of damage morphology with different pulse durations [3] indicated sharp steep edges produced by fs pulses, thus suggesting that "cold" fs ablation from solid to gaseous phase is possible without melting. In contrast with these observations, melting effects were also observed in dielectric coatings [4], thus indicating that liquid phase exists in fs damage formation at fluencies close to damage threshold. Time-resolved images of nanosecond [5] and femtosecond [6–10] damage formation were taken in the surface and bulk of bare materials and liquids. Despite the fact there has been several attempts to study nonlinear effects in thin films [11], imaging of fs damage formation was never studied on dielectric coatings with both temporal and spatial resolution, including phase and amplitude contrast at the same time. In this work, an experimental method of time-resolved digital holography (TRDH) [8,12] is employed to probe localized dynamics of thin film transformations as a response to ultrafast energy deposition by subpicosecond laser irradiation. To exemplify underlaying processes, tantala was used as the material of choice. Separate frames of an ultrafast movie representing the temporal evolution of fs breakdown morphology are presented. The results are supported with a numerical model based on the Kerr effect, electron rate equations, and Drude theory, which takes into account transient changes in the films and interference effects of the pump and probe pulses.

A set of Ta_2O_5 films was deposited by ion-assisted electron-beam deposition on super-polished fused-silica substrates. This technique is known to produce dense coatings with high optical quality. Four thicknesses of tantala coatings (4H, 2H, H, and H/2) were used for the experiments. Here H represents one-quarter wave of an optical thickness layer at 1030 nm. The refractive index for pump, a 1030 nm (and probe: 550 nm) wavelength was determined with a fitting procedure of the spectral reflectance and transmittance measurements: 4H: 2.10(2.17); 2H: 2.09(2.16); H: 2.10(2.17); H/2: 2.09(2.15).

A sketch of the experimental setup is shown in Fig. 1. An oscillator-amplifier Yb:KGW laser system ("Pharos" Light Conversion) was used to generate 300 fs pulses at a central wavelength of 1030 nm. The incoming pulses were split into a pump and probe branches by using a $\lambda/2$ plate and polarizing beam splitter (PBS). The pump pulse of fundamental wavelength was focused down to the 39 μm in effective diameter ($1/e$ level of max intensity) into the coating at the angle of incidence of 45 deg. The fluence level of the pump pulses was adjusted by the $\lambda/2$ plate and polarizer (P). Probe pulses were produced by amplifying and compressing spectrally broadened supercontinuum pulses using a noncollinear optical parametric amplifier (NOPA). NOPA was based on the BBO nonlinear crystal pumped by the third harmonic of the fundamental pulse [13]. After the amplification and the prism-based compression, bandwidth-limited probe pulses with 25 fs duration were produced at 550 nm central wavelength. The pump pulse was therefore much longer in time (300 fs) than the probe's.

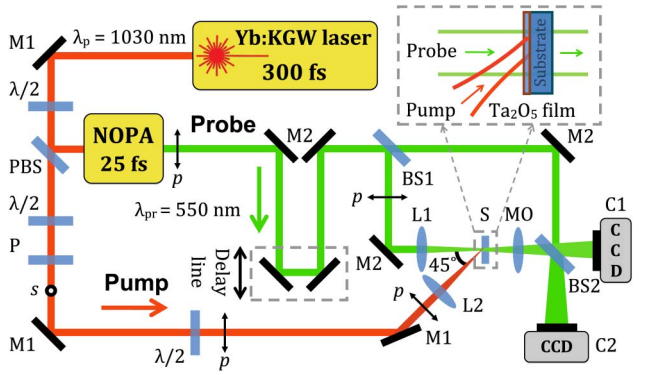

Fig. 1. Experimental setup for holographic registration of ultrafast processes in thin films: PBS, polarizing beam splitter; BS, beam splitter; P, polarizer; $\lambda/2$, half-wave plate; M, mirror; L, lenses; MO, microscope objective; S, Ta_2O_5 film sample; C1 and C2, digital CCD camera.

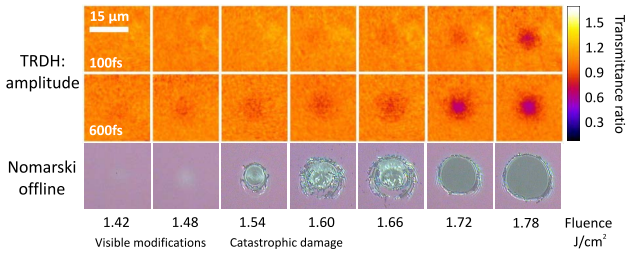

Fig. 2. Time-resolved amplitude contrast images (top rows) and postmortal Nomarski interference contrast images (bottom row) of surface morphology for H sample.

The compressed pulses were further used for probing the optically induced changes in thin film samples placed within the modified Mach–Zehnder interferometer [14]. A part of transmitted light (object wave) was collected by a microscope objective MO (20×, NA = 0.4), thus producing a magnified image of the sample in the plane of camera C2. Another part of the object wave was overlapped with a reference wave on camera C1 thus producing an interference pattern of a digital hologram. In both C1 and C2 cases, CCD sensors (1280×960 pixels with 3.75 μm pixel size) were used. Holograms were reconstructed numerically by so called convolution algorithm.

The energy fraction of the probe pulses was about 0.2% compared with the pump pulses. All this energy was required to overcome losses in the optical system and illuminate the CCD camera. The diameter of probe beam at the surface of the coating was at least 10 times larger than that of pump pulse; therefore fluence level of probing pulses was negligible. The sample was always translated after single-pulse irradiation to ensure each laser shot interrogates a fresh area.

First of all, the precise tuning of the zero-delay moment was carried out. It corresponds to conditions when maximal intensities of the pump and probe pulses are overlapped in time and positioned exactly at the front interface of the sample. It was found by complementary experiments measuring phase shift produced by the Kerr effect as a function of relative delay and fitting the corresponding data with Gaussian function. For better accuracy, pump fluence was set below LIDT. A total temporal uncertainty was estimated to be in the range of ±25 fs; it was limited by reproducibility of sample placement and duration of probe. Next the optical response of a film was investigated on sample "H" as a function of pump fluence. The results are shown in Fig. 2 for 100 and 600 fs probe delays. These timings corresponded to different stages of damage processes. At 100 fs delay, only a fraction of pump pulse has passed the coating while at 600 fs all possible energy is already deposited. An increase of pump energy resulted in observable losses of transmitted light for both delays. That is in agreement with findings of previous studies [7,15] where decrease in transmission is found as a result of free electron gas that absorbs and reflects the probe pulse. The basic process here is photoionization (PI) during the propagation of pulse through the coating. The impact ionization process becomes efficient when a sufficient electronic density is reached. Thus electronic avalanche is most likely taking place at the end of the pulse, which could explain the strong drop in transmission that we attribute to high free-electron density (note that the observations are in agreement with simulations). For 100 fs noticeable changes in transmittance occurring above 1.72 J/cm^2, which exceeds LIDT by roughly 15%, while for later time delays (600 fs) changes are visible for fluence as low as 1.48 J/cm^2. The fluence causing catastrophic damage was quite deterministic and always occurred at 1.51 J/cm^2 for the H sample. Damage criteria in this case was a crater visible by postmortal Nomarski microscopy (Fig. 2, bottom row). Noncatastrophic color changes were also observed below fluence of LIDT, and they are related to permanent modifications of the refractive index. The shape of the smoothly colored region correlated well with the electron excitation zone seen in amplitude images of TRDH. Such correlation indicates the effect of a localized high-energy electron heating of lattice acting as an initiating step of damage process. When increasing the fluence, we observe craters consisting of a melted and delaminated layer of the coating formed in a deterministic manner. In case of higher fluencies, the coating was completely removed.

Next, the optical response in single-layer coatings of four different thicknesses were investigated as a function of probe delay. A pump fluence was set slightly above LIDT (1.78 J/cm^2) thus every shot resulted in damage crater. Results of holographic imaging are illustrated in Fig. 3: the top row corresponds to amplitude changes that are proportional to relative transmission while bottom row indicates phase difference related to changes of refractive index. At least three distinct processes could be identified from the image sets. At the moment, when the pump pulse enters the coated surface (until first +200 fs), no changes in the amplitude images can be observed thus meaning no damage of tantala. However, an asymmetric negative response is observed in phase images. The geometry of experiments (45 deg pump and normal incidence of probe) explain such observation resulting in different thickness of Kerr affected zone within the bulk of substrate. Refractive index modifications induced by Kerr effect are instantaneous, which disappear immediately after the propagation. At the beginning, phase shift is produced mostly in fused-silica

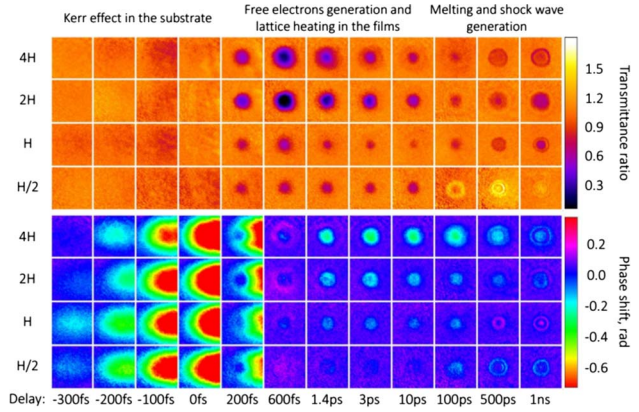

Fig. 3. Amplitude- (top row) and phase-contrast (bottom row) images of nonlinear excitation in tantala thin films corresponding to the four different samples.

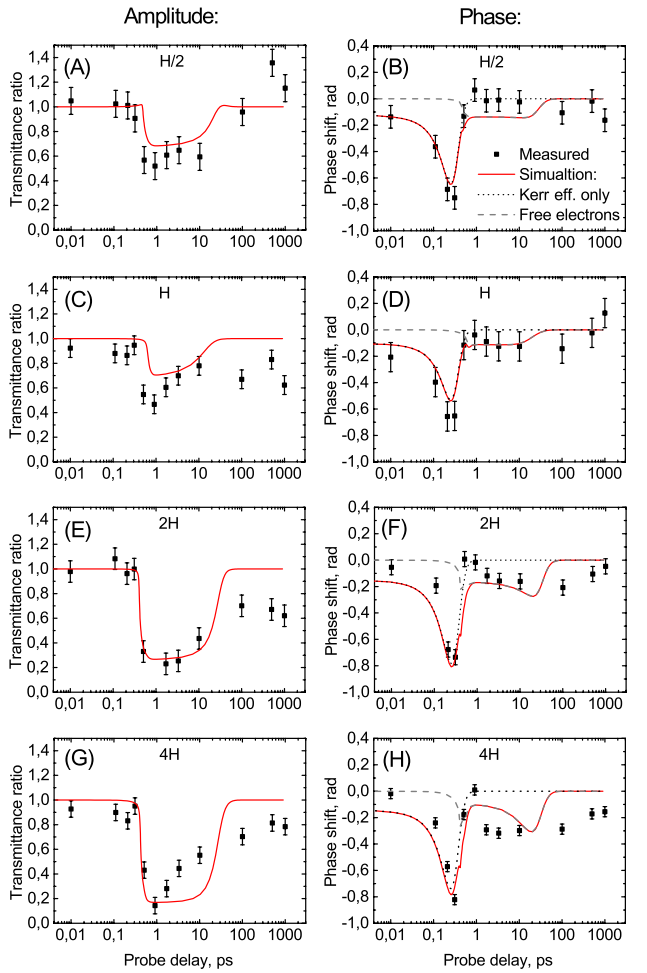

Fig. 4. (A), (C), (E), (G) Relative transmittance. (B), (D), (F), (H) Induced phase-shift evolution in time estimated at peak-intensity position of the coating. Rows correspond to deferent samples (H/2, H, 2H, and 4H). Red curve: overall phase shift. Dotted black curve: contribution of Kerr effect. Dashed gray curve: contribution from free electrons.

substrate because of longer optical path of Kerr zone compared to that of coating. Since it is an effect of the substrate, there are no significant differences among different samples. Only small variations are observed as a consequence of difference in coating thickness and transmission. At the moment when pulse is escaping the coating (+200 fs), nearly round patterns are visible in phase contrast. The same pattern is reproduced in the amplitude row, thus indicating the presence of excited free electrons. Note that highest changes in transmission are seen at the end of coating irradiation or slightly after, thus indicating the maximum of free-electron concentration at probe delays between +200 fs and +600 fs. Interestingly, the phase difference at maximal electron concentrations is almost negligible for the same probe delays. At later timing, negative phase shift is increasing, thus indicating distinct changes of refractive index related to thermal-energy deposition from high-energy electrons or generation of self-trapped excitons. This is associated with a decrease of the free-electron density and a relaxation of intensity drop in transmission. Ring-type modulations in refractive index start to occur at a time delay of 100 ps that could be attributed to fast growth of the internal pressure [16] and the birth of the shockwaves both in the sample [9,17] and air [10]. The quantitative results of obtained pictures are summarized in Fig. 4; here a constant of 250 fs was added to all delay data points in order to make them visible in the logarithmic scale.

For interpretation of experimental results, a numerical model was developed [18]. The model interprets coating as a system of sublayers with a spatial resolution of 10 nm and takes into account physical effects of light polarization, Fresnel reflections, interference, generation of free-electrons followed by relaxation processes inside every sublayer of the film. Phase shift in the substrate due to the Kerr effect was calculated separately: the nonlinear refractive index 4×10^{-16} cm^2/W of fused-silica (Suprasil) was used by integrating the phase shift along the probe's optical path. The fit of the experimental data resulted in a slightly higher nonlinear index than reported in the literature ($2–3.5 \times 10^{-16}$ cm^2/W [19]). Discrepancies are probable due to the Kerr effect of the film, which was not included in the model. A system of rate equations was solved for the every sublayer: rates of Keldysh photo-ionization, impact-ionization, and a relaxation were calculated in time and space. Free-carrier absorption of the whole optical system was calculated for every temporal iteration by considering the Drude model [7]. Temporal modulations of amplitude and phase were simulated for the probe wave at 550 nm. From the electron density distribution inside the film and its evolution in time, it was possible to reconstruct the dynamics of the refractive index profile. Calculations were done at the conditions of the experiment for the pump (fluence of 1.8 J/cm^2, P polarization, 45 deg AOI, pulse duration of 300 fs) and probe (550 nm, normal incidence). An effective electron mass of $0.5m_e$, a Drude relaxation time of 10^{-15} fs, and a decay term of 10 ps were used for calculations (see [18]). The obtained simulations of transmission coefficient ratio and phase delay are directly compared with experimental data in Fig. 4. Note that all parameters are the same for the different samples, except the thickness.

As shown, the numerical model with physical and bibliographic inputs reproduces the shape and order of

magnitude of the experimental curves. The first-order approximation indicates good understanding of the underlying Kerr effect and early electron-generation processes. The main difference between samples occur due to distinct coating thicknesses. First of all, the electric field intensity distributions are different. Second, induced phase and transmission changes are more strongly expressed in thicker coatings due to the longer path of propagation. Discrepancies in shapes of measured and simulated curves indicate that even more complex effects are involved at later probe delays. For example, +100–400 ps images indicate circular patterns that are similar to Newton rings. Such scenario is expected due to shockwave generation and its propagation into the air and substrate together with ejected material. Changes in sample object geometry cause deviation from the single-layer model.

In conclusion, it was shown that a time-resolved study based on the TRDH technique provides new insights into the dynamics of laser-induced damage formation of dielectric thin films. Processes occurring both in substrate (Kerr effect) and the coating (formation of free-electron plasma, interplay between melting, shockwave generation, and matter ejection) are directly visible at different time moments with good spatial and temporal resolution. Furthermore, quantitative data are obtained, which allow us to estimate physical sample properties with the evidence of distinct transient processes. A numerical model was adapted to simulate results of the TRDH experiment. The first-order approximation shows good understanding of the underlying early excitation processes triggering the damage. Nevertheless discrepancies in shapes of measured and simulated relaxation curves show limitations of the used rate-equation system during the ablation process.

The research has been supported by the Research Council of Lithuania (grant no. VP1-3.1-ŠMM-10-V-02-007), the European Social Fund Agency, and LASERLAB-EUROPE (grant no. 284464, EC's Seventh Framework Programme).

References

1. F. Quéré, S. Guizard, and Ph. Martin, Europhys. Lett. **56**, 138 (2001).
2. M. Mero, A. J. Sabbah, J. Zeller, and W. Rudolph, Appl. Phys. A **81**, 317 (2005).
3. B. N. Chichkov, C. Momma, S. Nolte, F. von Alvensleben, and A. Tünnermann, Appl. Phys. A **63**, 109 (1996).
4. A. Melninkaitis, T. Tolenis, L. Mažulė, J. Mirauskas, V. Sirutkaitis, B. Mangote, X. Fu, M. Zerrad, L. Gallais, M. Commandré, S. Kičas, and R. Drazdys, Appl. Opt. **50**, C188 (2011).
5. S. G. Demos, R. N. Raman, and R. A. Negres, Opt. Express **21**, 4875 (2013).
6. M. C. Downer, R. L. Fork, and C. V. Shank, J. Opt. Soc. Am. B **2**, 595 (1985).
7. D. Puerto, W. Gawelda, J. Siegel, J. Bonse, G. Bachelier, and J. Solis, Appl. Phys. A **92**, 803 (2008).
8. T. Balciunas, A. Melninkaitis, G. Tamosauskas, and V. Sirutkaitis, Opt. Lett. **33**, 58 (2008).
9. Y. Hayasaki, M. Isaka, A. Takita, and S. Juodkazis, Opt. Express **19**, 5725 (2011).
10. A. Urniežius, N. Šiaulys, V. Kudriašov, V. Sirutkaitis, and A. Melninkaitis, Appl. Phys. A **108**, 343 (2012).
11. L. Zhu, C. Zhou, T. Wu, W. Jia, Z. Fan, Y. Ma, and G. Niu, Appl. Opt. **49**, 2510 (2010).
12. T. Balciunas, A. Melninkaitis, A. Vanagas, and V. Sirutkaitis, Opt. Lett. **34**, 2715 (2009).
13. N. Šiaulys, V. Kudriašov, T. Stanislauskas, T. Malinauskas, A. Urniežius, and A. Melninkaitis, Opt. Lett. **37**, 4916 (2012).
14. E. Cuche, P. Marquet, and C. Depeursinge, Appl. Opt. **38**, 6994 (1999).
15. T. Q. Jia, H. Y. Sun, X. X. Li, D. H. Feng, C. B. Li, S. Z. Xu, R. X. Li, Z. Z. Xu, and H. Kuroda, J. Appl. Phys. **100**, 023103 (2006).
16. D. S. Ivanov, Z. Lin, B. Rethfeld, G. M. O'Connor, T. J. Glynn, and L. V. Zhigilei, J. Appl. Phys. **107**, 013519 (2010).
17. M. Sakakura, M. Terazima, Y. Shimotsuma, K. Miura, and K. Hirao, Opt. Express **15**, 5674 (2007).
18. L. Gallais, B. Mangote, M. Commandré, A. Melninkaitis, J. Mirauskas, M. Jeskevic, and V. Sirutkaitis, Appl. Phys. Lett. **97**, 051112 (2010).
19. F. Billard, "Métrologie de l'indice non-linéaire dans les verres en régime nanoseconde, picoseconde et sub-picoseconde," Ph.D. thesis (Université Paul-Cézanne Aix-Marseille III, 2005).